

Multi-seeded multi-mode formation of embedded clusters in the RMC: Structured star formation toward the south-east boundary

J. Z. Li^{1,2} & M. D. Smith²

¹*National Astronomical Observatories, Chinese Academy of Sciences, 20A Datun Road, Chaoyang District, Beijing 100012, China; ljz@bao.ac.cn*

²*Armagh Observatory, College Hill, Armagh BT61 9DG, N. Ireland, UK; mds@arm.ac.uk*

ABSTRACT

The Rosette Molecular Complex contains embedded clusters with diverse properties and origins. We have previously explored the shell mode of formation in the north (Regions A & B) and the massive concentrations in the ridge (Region C). Here, we explore star formation towards the south of the complex, Region D, based on data from the spatially complete 2 Micron All Sky Survey. We find that stars are forming prolifically throughout this region in a highly structured mode with both clusters and loose aggregates detected. The most prominent cluster (Region D1) lies in the north-center. This cluster is over 20 pc to the south of the Monoceros ridge, the interface of the emerging young OB cluster NGC 2244 with its ambient molecular clouds. In addition, there are several branches stemming from AFGL 961 in Region C and extending to the south-east boundary of the cloud. We invoke a tree model to interpret this pattern, corresponding to probable tracks of abrupt turbulent excitation and subsequent decay. Alternatively, we discuss gravoturbulent collapse scenarios based on numerical simulations. Relative stellar ages and gas flow directions will differentiate between these mechanisms.

Subject headings: ISM: Clouds – Infrared: stars – Stars: formation – Stars: pre-main sequence – ISM: structure

1. Introduction

The Rosette Molecular Cloud (RMC) is known as one of the most massive giant molecular complexes (GMCs) in the Galaxy (Blitz & Thaddeus 1980). At a distance of ~ 1.5 kpc, it is among the most prominent sites for the exploration of active star formation (Cox, Deharveng & Leene 1990; Block, Geballe & Dyson 1993). Indeed, the presence of several clusters of young stars associated with massive clumps were recognised on near-infrared K-band images (Phelps & Lada 1997). Li & Smith (2005a) were able to probe the clusters in more detail by using the three-band spatially complete 2 Micron All Sky Survey (2MASS). They showed that deeply-embedded clusters, sub-clusters and loose aggregates are widely distributed throughout the RMC.

Cluster formation in the RMC is taking place in a multi-seeded manner i.e. clusters are forming in parallel yet in independent locations (Li & Smith 2005a). There is also strong evidence for multi-mode formation, with the mode related to the cloud location. Four regions were identified by Li & Smith (2005a) as also indicated here in the upper panel of Fig. 9.

Firstly, Regions A & B were identified with the interaction layer of the Rosette Nebula with swept-up and fragmented arcs of molecular gas (Li & Smith 2005b). The interface contains several loose aggregates spread along the compressed cloud layers. In Region C, a burst of formation of compact sub-clusters and high-mass stellar groups, signifying new generations of OB cluster formation, is taking place (Li & Smith 2005c). Region C is associated with the densest ridge of the RMC.

Star formation in the RMC that has previously taken place (Blaauw 1964; Singh & Naranan 1979; Turner 1976) or is now proceeding (Li & Smith 2005a) could well be consistent with the scenario of sequential formation of massive clusters in GMCs (Elmegreen & Lada 1977; Lada 1987). If the choice is between spontaneous and triggered collapse, then the latter has considerable support. However, the specific modes and mechanisms to be held responsible in the contrasting areas remain to be determined. In this paper, we will focus on the embedded population of young stars in Region D, toward the south-east boundary of the RMC. At a distance exceeding 20 pc from the interaction layer, the influence from the emerging young open cluster NGC 2244 and its associated HII region is very limited (Cox, Deharveng & Leene 1990; Schneider, Stutzki & Winnewisser et al. 1998). On the other hand, being in the vicinity of the massive young stars in Region C, regions of rapid dispersal and strong compression might be evident. Therefore, exploration of Region D may offer a critical test of the conventional understanding of sequential cluster formation (Lada 1987).

2. Data Acquisition & Analysis

A detailed review of the methodology was presented in the first of this series (Li & Smith 2005b). We employ color constraints to substantiate the embedded nature of the clusters. Control fields were utilised to help determine the proportions of embedded and background stars.

Both archived data from the 2MASS Point Source Catalogue (PSC) and the IRAS Sky Survey Atlases (ISSA) were retrieved via IRSA (<http://irsa.ipac.caltech.edu/>). For a detailed introduction to the 2MASS mission and the 2MASS PSC, please consult the 2MASS Explanatory Supplement. The 2MASS PSC contains 470 million source extractions with a broad range of photometric quality. Restrictions to the 2MASS photometric data are necessary to meet the requirements of different studies. Here, we extract only those sources with certain detections in all three near infrared bands: J, H and Ks. We then further restrict the Ks band signal to noise ratio to be above 15, to constrain stars in the control fields to the unreddened main-sequence and post-main-sequence tracks on the (J-H) to (H-Ks) diagram (see Fig. 4a of Li & Smith (2005b)).

3. Spatial distribution of embedded clusters and loose aggregates

The spatial distribution of the Region D sample sources are plotted as a function of H-Ks color in Fig. 1. The color distinction helps to eliminate a possible random distribution of foreground field stars without excluding potential cloud members which may also be widely distributed. Reddened sources with a H-Ks color above 0.5 and 0.7 are overplotted onto the distribution of optical depth at 100 μm (upper panel) and cold dust temperature (lower panel), respectively, as derived from the ISSA data (Li & Chen 1996). Clustering and fine structure in the distribution begin to appear as the minimum H-Ks reddening is increased.

A dense cluster is readily seen to the north of the center of this region, Region D1. This sub-cluster possesses a symmetric and compact structure, as does the associated molecular clump (Blitz & Thaddeus 1980; Williams, Blitz & Stark 1995). We could expect D1 to be the result of largely spontaneous or non-triggered cluster formation, rather than having been primarily induced by the expanding Rosette Nebula and its embedded OB cluster NGC 2244. The spatial separation of more than 20 pc between Region D1 and the Monoceros ridge provides support for this argument, consistent with the claims made by Blitz & Thaddeus (1980). In addition, ultraviolet ionization of the inter-clump gas is probably insufficient to induce implosion of the clumps at and beyond this distance (Blitz & Thaddeus 1980; Cox, Deharveng & Leene 1990; Schneider, Stutzki & Winnewisser et al. 1998) despite the large clump to inter-clump density contrast detected in the RMC (Blitz & Thaddeus 1980; Williams, Blitz & Stark 1995). This issue will be further elaborated in § 7.

We cannot state unequivocally which of the reddened stars are embedded and which are background through just the stellar distribution. However, several lanes of reddened sources and widely distributed aggregates are discernible in Region D. In Fig. 1, these regions are outlined by either circles or rectangles according to their appearance. Some of the stellar concentrations are known to be associated with IRAS sources (Cox, Deharveng & Leene 1990) and young stellar groups (Phelps & Lada 1997). This provides first evidence that the majority of the reddened sources associated with the regulated structures are embedded in the cloud, rather than resulting from reddening of background stars. Nevertheless, in areas of clustering other than D1, no major gas clumps as prominent as those located in Region C exist (Williams, Blitz & Stark 1995), as also indicated by the optical depth distribution (upper panel). Some aggregates can be traced to regions with comparatively low opacity, beyond the filaments in the extension of the RMC detected in lines of CO & C¹³O (Williams, Blitz & Stark 1995). This further reduces the attribution of the clustered appearance of the reddened sources in Region D to the effects of cloud extinction and reddening on randomly distributed background stars. On the other hand, certain stellar groups are associated with relatively warm dust temperatures of 25-41 K (lower panel), which may be a factor related to their gestation or to the heating by massive embedded stars.

To measure the significance of the clustering of the candidate young stars in Region D and particularly those associated with Region D1, we have computed the standard two-point correlation

function. We first determine the number of stellar pairs, $H_d(\theta)$, separated by an angle θ , thrown into logarithmic bins between $\log(\theta)$ and $\log(\theta) + d\log(\theta)$. This is compared to the predicted distribution for a random sample of stars spread over the same area, $H_r(\theta)$. The two-point correlation function is then defined as

$$\Phi(\theta) = \frac{H_d(\theta)}{H_r(\theta)} - 1. \quad (1)$$

Hence, a random distribution yields $\Phi = 0$. Such a random distribution is found in Fig. 2 only when we take all the stars with H-Ks > 0.2 mag in the entire Region D (dashed line).

As demonstrated in Fig. 2, the higher the (H-Ks) color constraint placed on the sample of sources, the stronger the resultant spatial correlation and, hence, the clustering of sources. This holds for both the entire region and the sub-cluster (Fig. 3). In fact, the values of Φ uncovered here are significantly larger than found in other clusters in the Rosette Complex (maximum values of ~ 6 (A), 0.5 (B) and 1.5 (C) were found).

Two important results emerge on re-plotting the number Φ logarithmically, as shown in Fig. 4. Firstly, the correlation functions are consistent with power-laws. This implies that *there is no particular scale length which we could identify with either a Jeans length or other fragmentation scale*.

Secondly, the correlation function is steep. The Φ - θ power-law index is $\gamma \sim -0.84$ for the samples with H-Ks > 0.7 mag in Region D and $\gamma \sim -0.95$ in Region D1, as indicated by the dot-dashed line segments. The function is steep in comparison both to other regions of the RMC (Li & Smith 2005b,c) and to other clusters (e.g. Scalo & Chappell 1999). Hence, clustering is particularly strong here suggesting that these stars are *either tightly bound or extremely young*. We can ask if the strong correlation on the fine scales may be partly due to the distribution of sources into the branches discussed below. However, it is clear that the branches are quite wide (of order of 0.2°) and we find no particular length scale that could be associated with this width.

The distribution of projected separation distances between nearest neighbours contains distinct information. While the two-point correlation function describes the nature of the hierarchical clustering, the nearest neighbour distribution will emphasise the presence of any scale of fragmentation or a scale associated with gravitational confinement. The left panel of Fig. 5 demonstrates an almost perfect agreement with a random distribution for the entire sample with H-K exceeding 0.2. In contrast, for the deeply embedded stars (the right panel), there is a significant excess of neighbouring stars with a separation of $\sim 30''$ and a second possible excess at $\sim 55''$. Given the broad distribution expected for a random sample, this is more plausibly interpreted as a deficit of separations of ~ 40 – $45''$, corresponding to a scale of 0.3 parsec. Given the size of the error bars, however, we just note here that there is an indication of a scale length which may correspond to that of clump fragmentation into massive stellar binaries.

4. Color-Color Diagrams

To explore the nature of the candidate young stars in Region D and particularly Region D1, all 2MASS sources that match the sample selection criteria introduced in § 2 are put onto (J–H)—(H–Ks) diagrams (Fig. 6). Color-color diagrams for two off-cloud control fields were constructed as a comparison (Li & Smith 2005b) which indicate negligible foreground and background extinction generally toward the RMC field.

Considerable fractions of the reddened sources are found to be located to the right of the reddening band of normal field stars in the Region D diagram. The fractions are nearly one third and a half for the sources with H-Ks above 0.5 and 0.7 mag, respectively. The infrared excesses indicate their youth, and provide support that the very young stars in Region D are associated with the molecular cloud.

Nevertheless, contamination by background field stars in this region is high due to the comparatively low extinction at the south-east boundary of the RMC (Blitz & Thaddeus 1980; Williams, Blitz & Stark 1995) and the large sky area involved. Indeed, a clear concentration of reddened sources are located to the left edge of the reddening band and these are probably not cloud members. Due to their position in the reddening band, the majority of these sources could well be background giants. The visual extinction in this region is found to range from ~ 0.5 to 24.5 mag and indicates a mean of ~ 4 mag.

The most extreme source in the Region D diagram is identified as a heavily reddened source invisible in the optical. Its position in the diagram suggests a pre-main sequence origin of the object.

Inspection of the color-color diagram for Region D1 reveals no clear concentration of reddened sources in the reddening band. About 20% of the reddened sources are located to the right of the reddening band for normal stars and are probably intermediate and low mass young stars with intrinsic excess emission. The sub-cluster shows a maximum visual extinction of roughly 20 mag. However, we find no evidence for protostars with high infrared excesses in this sub-cluster, indicating that very massive stars are not currently forming in this specific region.

5. Color-Magnitude Diagrams

Color-Magnitude Diagrams (CMD) are presented in Fig. 7. The near-vertical solid line represents the loci of stars on the unreddened main-sequence. A clear separation between the foreground main sequence stars and the candidate cluster members is apparent.

About one sixth of the candidate cluster members are located above the reddening vector drawn for a A0 dwarf. This indicates that a considerable number of sources might be massive protostars still deeply immersed in their parental cloud cores or envelopes. The location of the

most extreme source among these is indicated by a diamond. It can be a pre-main sequence star as massive as $\sim 50 M_{\odot}$ and is the most massive candidate young stellar object in this region. Region D is thus associated with a structured distribution of loose aggregates containing massive young stars.

The compact sub-cluster residing in Region D1, as indicated by the CMD, is probably a medium mass embedded cluster. The most massive candidate young stars have ultimate masses of below or around $20 M_{\odot}$. Nearly one third of the candidate cluster members in this region are located above the reddening vector of a A0 dwarf and are good candidates for intermediate mass young stars.

Some sources are easily detected in the H and Ks bands but are overlooked in the J band, mainly due to the sensitivity of the J-band detection to extinction along the line of sight (Kaas, Olofsson & Bontemps 2004). Other possible reasons for exclusion include (i) being shrouded by apparently bright sources associated with or nearby in projection and (ii) severely obscured from identification by diffuse emission. Therefore, the strict sample selection method employed, along with the flux and resolution limited 2MASS survey, directly result in the omission of many sources well measured in only the H and Ks bands. These sources were also accumulated and are presented on the CMDs of Regions D and D1 (plus signs). This shows evidence that these criteria missed sources are predominantly candidates for embedded young stars suffering high extinction. High-resolution, high sensitivity surveys are therefore required to perform a complete census of the embedded population.

6. Ks Luminosity Function

The luminosity function of embedded clusters is usually employed as a tool to address questions related to the initial mass function. The Ks luminosity functions (KLF) for Region D and Sub-region D1 are presented in Fig. 8. Both KLFs correspond well to a power law distribution in the range of $11.0 < Ks < 14.5$ mag. They show a consistent slope of ~ 0.4 and, consequently, suggest a young age of < 1 Myr when compared with embedded clusters of known ages (Lada & Lada 1995). The embedded cluster in Region D thus has an indicated age comparable to that of the Region C cluster.

A comparison of the KLF of each well-confined region of star formation in the RMC provides a consistent view of sequential star and cluster formation. The young open cluster NGC 2244 with an age of around 2 Myrs is acknowledged to represent the oldest episode of recent cluster formation in the RMC (Li 2005). Clusters in the swept-up shells of the expanding HII region are subsequently formed, possessing ages of > 1 Myr and are still closely associated with their birth sites (Li & Smith 2005b). Embedded clusters hatched in both Regions C & D have KLF-indicated ages of the order of < 1 Myr and so are among the most recently formed. However, although there is an age sequence from north to south, it does not necessarily mean that the Region C & D clusters are exclusively triggered by NGC 2244, as we now discuss.

7. Schematic models

An entire view of the reddened stars in the RMC is provided in Fig. 9a. The distribution of the sub-clusters in Regions C & D surprisingly resembles an ‘upside-down tree’ that is rooted at the center of Region C. There are four prominent branches traced with solid lines. Remarkably, the IRAS 60 μm map of this region (Fig. 9b) also displays extensions in flux with a similar pattern in accordance with the regulated distribution of the reddened sources. We can exclude its origin as due to monotone tracking problems of the IRAS survey since the flux pattern of dust emission is elongated and oriented in different directions.

There are at least three potential causes for the structured star formation in Region D. Firstly, in the **internal sequential** scenario, the emerging young OB cluster in the north, NGC 2244, triggers new generations of massive star formation in the densest ridge of the RMC (Li & Smith 2005c). These stars then trigger further generations, finally reaching the south-eastern tip of the cloud. Note that the trigger mechanism is clearly compression associated with the HII region for clusters A & B embedded in the interface but the impact of shocks further into the cloud should be severely impeded by the swept-up shells (Li & Smith 2005b). Deep into the molecular cloud, radiative implosion has been discussed as a possible mechanism by Schneider, Stutzki & Winnewisser et al. (1998), who find that the incident far-ultraviolet flux is low in the RMC as compared to other star formation regions, though its partial contribution to the active star formation in the south-east of the RMC cannot be excluded.

On the other hand, Cox, Deharveng & Leene (1990) present evidence that radio continuum emission extends almost a degree to the south from the main cluster NGC 2244 in the direction from the Monoceros ridge toward AFGL 961. This indicates that the cloud ridge could be compressed by the H₁₈OH II region from behind the cloud. However, the radio emission overlapping with AFGL 961 is extremely weak and absent further to the south. It is difficult to argue that ionization associated with the H₁₈OH II region could significantly raise the pressure and be the primary trigger of the collapse of molecular clumps associated with the compact clusters in Region D.

Secondly, **external triggering** should be considered. The compression, fragmentation and collapse may be associated with an old supernova or with the Perseus Arm (Guseva, Kolesnik & Kravchuk 1984; Perez 1991). The branches then represent the compressed filaments which follow the decay of macroturbulence. On the other hand, Region D sits at the base of the ‘relic’ tail of the RMC that may have resulted from tidal force dissipation during its interaction with the Galactic plane. This can be the reason why clustered star formation is taking place in this specific region along the Perseus Arm, where the general gas density is comparatively low. This could also be related to how the tree-like structure and, consequently, the Region D sub-clusters and loose aggregates were formed.

Once externally triggered, a giant cloud is expected to undergo *gravoturbulent collapse* (Klessen & Burkert 2001). This implies that the cloud material collapses into sheets. Flow within the sheets leads to the formation of filaments. Mass accumulates where the filaments intersect, enhanced by the

self-gravity. Very high mass stars may then form in the high mass clump at the intersection. Other massive stars form within the dense filaments. As the intersection location moves, new adjacent clusters containing high mass stars form. This global collapse should produce the youngest massive stars in the central agglomeration, consistent with the observed state of the RMC.

Finally, we consider a **tree model**, in which star formation proceeds from the inside, out along the branches, as an alternative mechanism. The formation of the structure is interpreted as directly triggered by the proto-O triple system at the south-center of Region C (Li & Smith 2005c), the location of which seems to match well the root of the tree. Note that an additional branch of the tree structure seems to exist extending from the massive multiple system associated with AFGL 961 to the eastern edge. Both the compact sub-clusters in Region C and the loose aggregates in Region D can be triggered by the violent activity related to the formation of the protostellar O stars. Thus, the tree structure is here attributed to strong activity associated with the high-mass star formation in Region C. The induced large-scale turbulence compresses the edges of the cloud and then decays along radial directions, leading to systematic star formation along sheet-like structures.

Nevertheless, several less conspicuous far infrared emission cores also exist and are extensively scattered within Region D. They have locations commensurate with the distribution of molecular clumps or filaments (Williams, Blitz & Stark 1995). Each is more or less spatially associated with a loose aggregate of reddened young stars, providing support to our remarks that recent clustered star formation is occurring in this region. However, the structured distribution of candidate young stars does not end where the clumps or filaments do. This suggests that the tracks of star formation correspond to locations where the turbulence has decayed and the gas has been efficiently transformed into stars.

8. Summary

Reddened stars are distributed within clusters, loose aggregates and filaments towards the south-east boundary of the RMC. The clustering is relatively strong in Region D, as measured by the two-point correlation function. This suggest that the stars have not had time to disperse, possibly commensurate with a very young age, as testified by the KLFs. Supposing a velocity dispersion of 2 km s^{-1} , the stars would disperse within a region of size 4 pc after 1 Myr. At a distance of 1.5 kpc, this corresponds to 0.16° . This is roughly consistent with the widths of the branches along which the reddened stars are aligned. After 2 Myr, however, the branches would be hard to discern.

Schematic models are presented which help elucidate the nature of clustered star formation throughout the south-east quadrant of the RMC. A scenario of extensive clustered star formation induced by the violent activity of the newly hatched proto-O stellar group associated with AFGL 961, from where the branches appear to stem, is suggested. This tree model, in which the

central roots form before the branches, contrasts with the gravoturbulent model, in which material flows inwards along sheets and filaments, accumulating in the massive central ridge.

How can we differentiate between these two contrasting models? Firstly, we can explore the gas flows within the RMC to gain evidence for inflow or outflow. At present, it is known that turbulent motions dominate the dynamics, with the addition of a moderate large-scale velocity gradient (Williams, Blitz & Stark 1995). Secondly, we could derive more accurate ages for the young stars. If, as supported by the presence of two powerful molecular outflows (Schneider, Stutzki & Winnewisser et al. 1998), the massive clusters along the ridge are indeed the youngest, then the gravoturbulent model would be difficult to challenge.

Acknowledgments

Beside the 2MASS Archive, this work also made use of IRAS PSC & ISSA data. DSS Survey data (STSCI, funded by NSF) were also employed. This project is sponsored by SRF for ROCS, SEM and is partially supported by the Department of Culture, Arts and Leisure (Northern Ireland) and PPARC (U.K.).

REFERENCES

- Bessel, M. S. & Brett, J. M., 1988, *PASP* 100, 1134
- Blaauw, A., 1964, *ARA&A* 2, 213
- Blitz, L. & Thaddeus, P., 1980, *ApJ* 241, 676
- Block, D. L., Geballe, T. R. & Dyson, J. E., 1993, *A&A* 273, L41
- Cox, P., Deharveng, L. & Leene, A., 1990, *A&A* 230, 181
- Elmegreen, B. G., & Lada, C. J., 1977, *ApJ* 214, 725
- Guseva, N. G., Kolesnik, I. G., Kravchuk, S. G., 1984, *SvAL* 10, 309
- Kaas, A. A. Olofsson, G. & Bontemps, S. et al. 2004, *A&A* 421,623
- Klessen, R. S., & Burkert, A. 2001, *ApJ*, 549, 386
- Lada, C. J., 1987, *IAU Symp.* 115, *Star Forming Regions* (Dordrecht: Reidel), Eds: M. Peimbert & J. Jugaku, 1
- Lada, C. J. & Lada, E. A., 1995, *AJ* 109, 1682
- Lejeune, T. & Schaerer, D. 2001, *A&A*, 366, 538
- Li, J. Z. & Chen, P. S., 1996, *Chinese Astro. & Astroph.* 20, 445

- Li, J. Z., 2005, ApJ, 625, 242
- Li, J. Z. & Smith, M. D., 2005a, ApJ, 620, 816
- Li, J. Z. & Smith, M. D., 2005b, A&A, 431, 925
- Li, J. Z. & Smith, M. D., 2005c, AJ 130, 721
- Meyer, M. R., Calvet, N., Hillenbrand, L. A., 1997, A&A, 114, 288
- Perez, M. R., 1991, RMxAA 22, 99
- Phelps, R. L. & Lada, E. A., 1997, ApJ 477, 176
- Rieke, G. H. & Lebofsky, M. J., 1985, ApJ 288, 618
- Scalo, J. & Chappell, D. 1999, ApJ 510, 258
- Schneider, N., Stutzki, J. & Winnewisser, G. et al. 1998, A&A, 335, 1049
- Singh, K. P. & Naranan, S., 1979, Ap&SS 66, 191
- Stanke, T., Smith, M. & Gredel, R. et al. 2005, A&A subm.
- Turner, D. G., 1976, ApJ 210, 65
- Williams, T. P., Blitz, L., Stark, A. A., 1995, ApJ 451, 252

Fig. 1.— The spatial distribution of the Region D sub-clusters and aggregates with $(H-Ks) > 0.5$ (upper panel) and > 0.7 (lower panel), respectively. Note that the source distribution of reddened sources is overplotted onto the distribution of optical depth at $100 \mu\text{m}$ in the upper panel and onto that of the color-temperature in the lower panel. The distribution of optical depth and cold dust temperature was calculated from IRAS $60 \mu\text{m}$ and $100 \mu\text{m}$ images (Li & Chen 1996).

Fig. 2.— The two-point correlation function for objects in Region D of the RMC. The three lines correspond to the data with $H-Ks > 0.2$ mag (dashed line, 2660 stars), $H-Ks > 0.5$ mag (dotted line, 792) and $H-Ks > 0.7$ mag (solid line, 295 stars). The inset displays the spatial distribution of the sample sources with $H-Ks > 0.5$ mag within the entire area of $1.23^\circ \times 0.64^\circ$.

Fig. 3.— The two-point correlation function for objects in the circular Sub-Region D1 of the RMC. The three lines correspond to the data with $H-Ks > 0.2$ mag (dashed line, 313 stars), $H-Ks > 0.5$ mag (dotted line, 166) and $H-Ks > 0.7$ mag (solid line, 74 stars). The inset displays the spatial distribution of the sample sources with $H-Ks > 0.5$ mag within the area of diameter 0.32° .

Fig. 4.— The $\log(\Phi)$ - θ correlation for Region D (upper panel) and Region D1 (lower panel). A power-law correlation function is thus linear here. The dot-dashed straight lines correspond to power-laws of the form $\Phi \propto \theta^{-0.84}$ (upper panel) and $\Phi \propto \theta^{-0.95}$ (lower panel). The full and dotted data lines correspond to the definitions employed in Figs. 2 and 3.

Fig. 5.— The number distribution of the projected separation distance between nearest neighbours for Region D. As indicated, the panels correspond to the star samples with $H-Ks > 0.2$ mag (2660 stars), $H-Ks > 0.5$ mag (792) and $H-Ks > 0.7$ mag (295 stars). The solid lines are the equivalent distributions for the same numbers of randomly distributed stars within the same area. Error bars are calculated from square-root number statistics.

Fig. 6.— Color-color diagrams of the Region D cluster and its sub-cluster D1. Candidate cluster and sub-cluster members are denoted as dots. The source with the highest $H-Ks$ in the Region D diagram is indicated by a diamond. Solid lines represent the loci of the main-sequence dwarfs and giant stars (Bessel & Brett 1988). The arrow in the upper left of the plot shows a reddening vector of $A_v = 5$ mag (Rieke & Lebofsky 1985). The dotted dashed line indicating the locus of de-reddened T Tauri stars (Meyer, Calvet & Hillenbrand 1997). The dashed lines define the reddening band for the normal stars and T Tauri stars, and are drawn parallel to the reddening vector; crosses were overplotted with an interval corresponding to 5 mag of visual extinction.

Fig. 7.— Color-magnitude diagrams of the Region D cluster and its sub-cluster D1. Source indicators are the same as Fig. 6. Sources missed by the selection criteria are plotted with plus signs. The unreddened main-sequence is plotted as a solid line (Lejeune & Schaerer 2001). The slanted line with an arrow at the tip denotes a reddening of $A_v = 20$ mag of an A0 type dwarf.

Fig. 8.— The KLF of the Region D cluster (solid line) and its sub-cluster D1 (dotted line). It is evident that both Regions D and D1 have a very similar slope of ~ 0.4 in the range of $11.0 <$

$K_s < 14.5$ mag, signifying that the embedded sub-clusters have ages of only < 1 Myr and are still engaged in their early stages of evolution.

Fig. 9.— Upper panel: The structured distribution of the embedded clusters and loose aggregates of candidate young stars in the entire RMC. A tree pattern is schematically illustrated by the thick continuous lines overlaid. Lower panel: An intriguing distribution of the IRAS $60\ \mu\text{m}$ emission of the RMC that matches quite well the star formation branches.

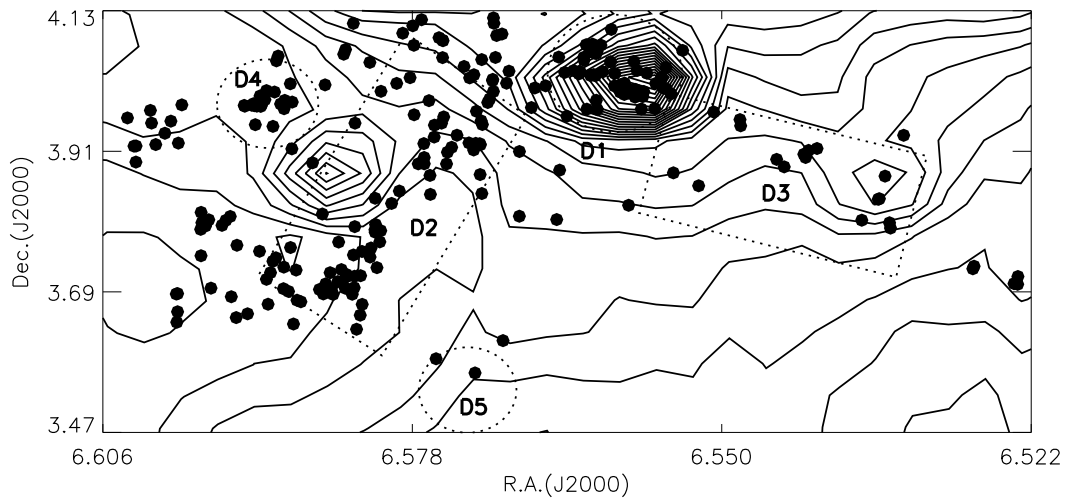
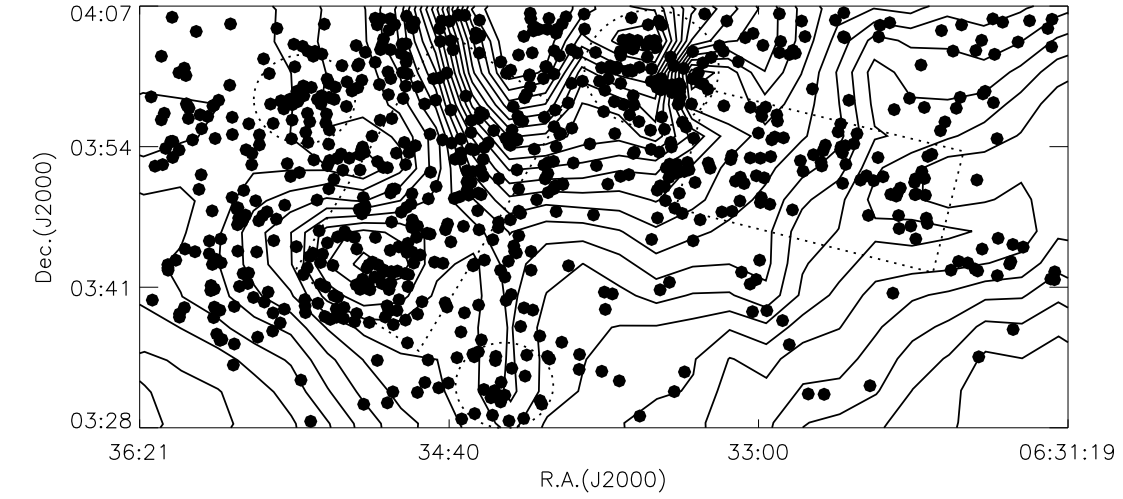


Fig.1

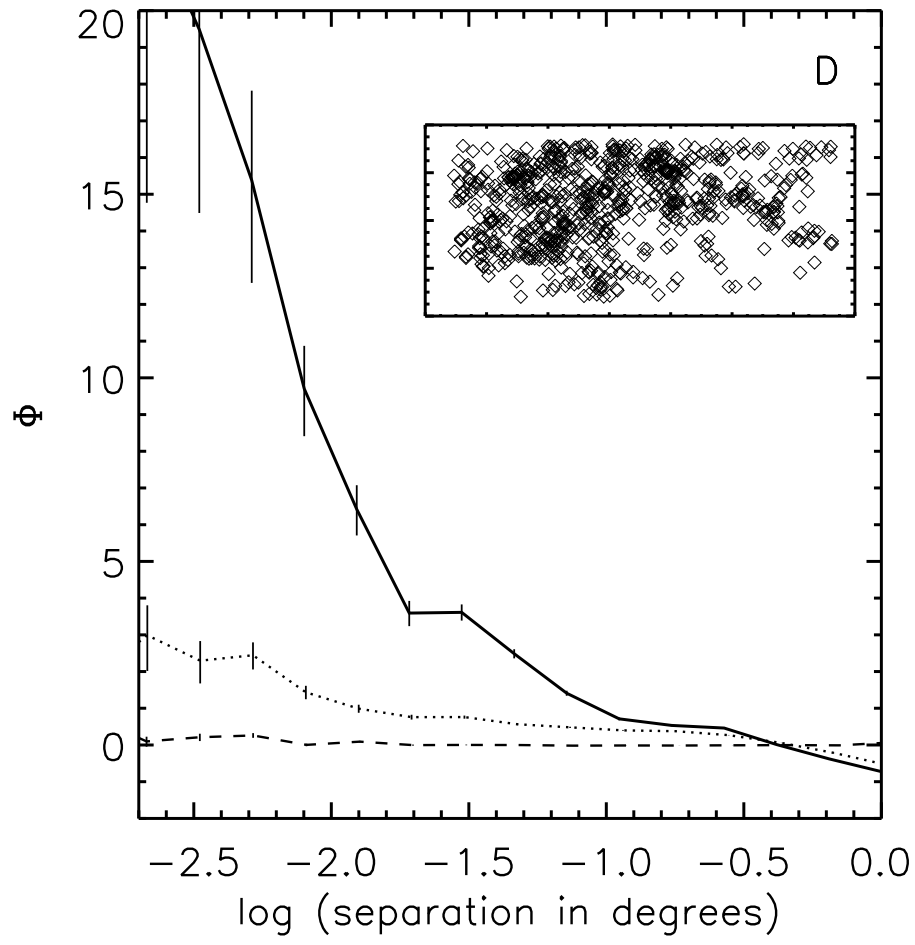


Fig.2

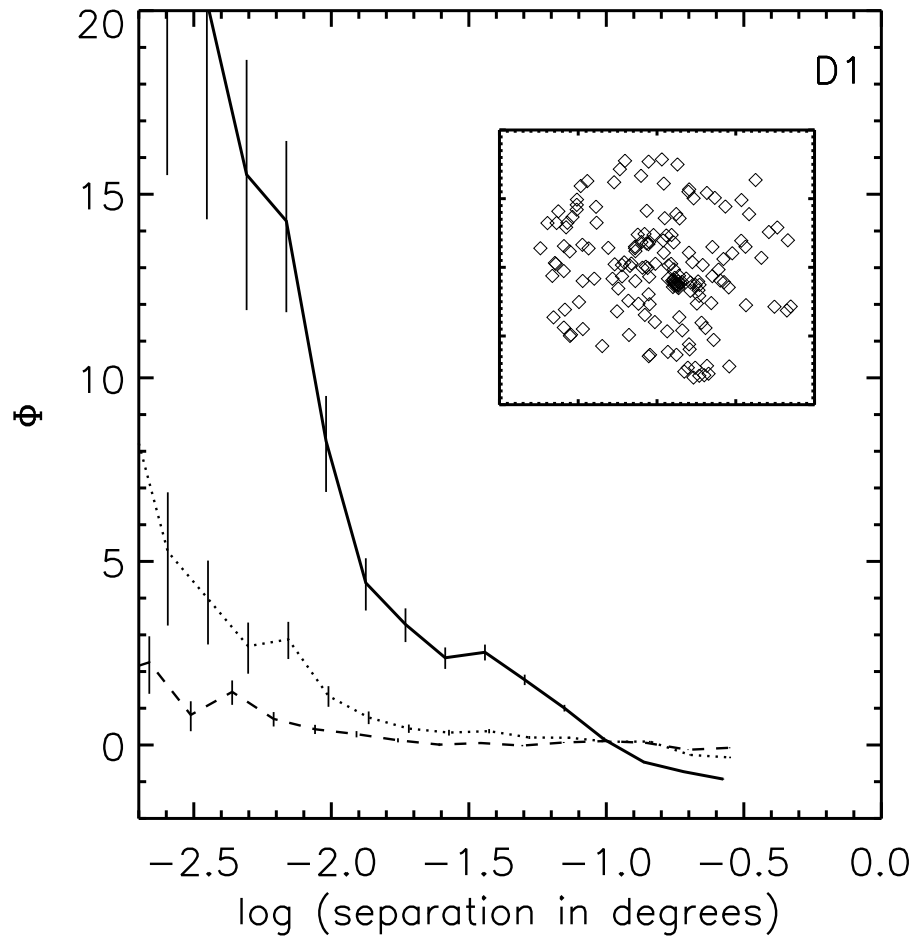
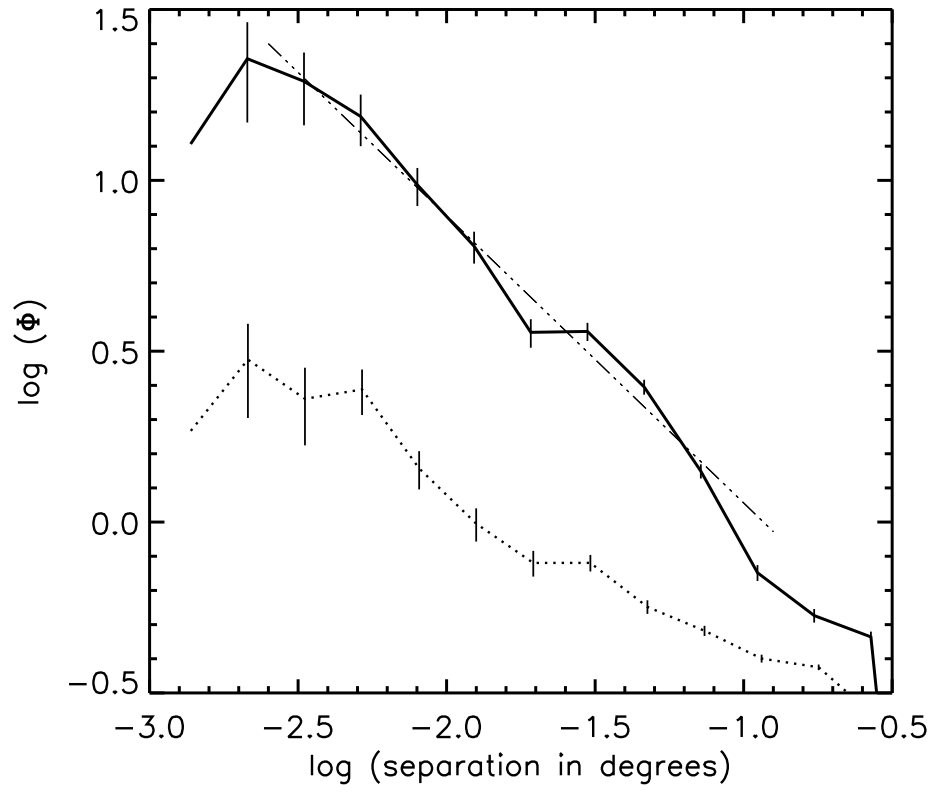


Fig.3



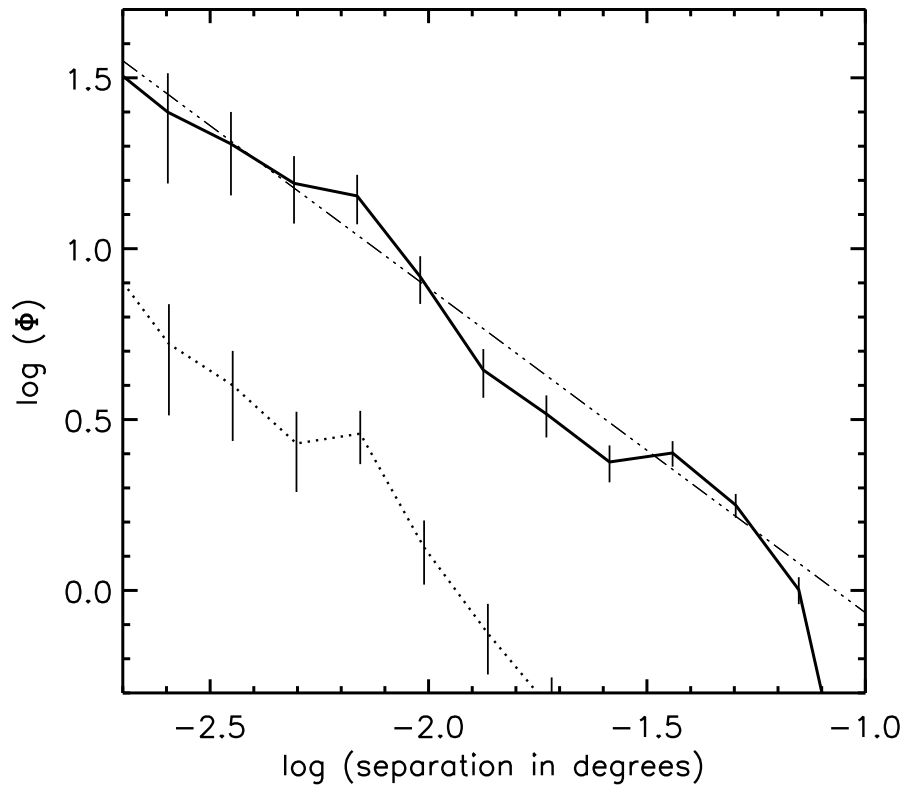
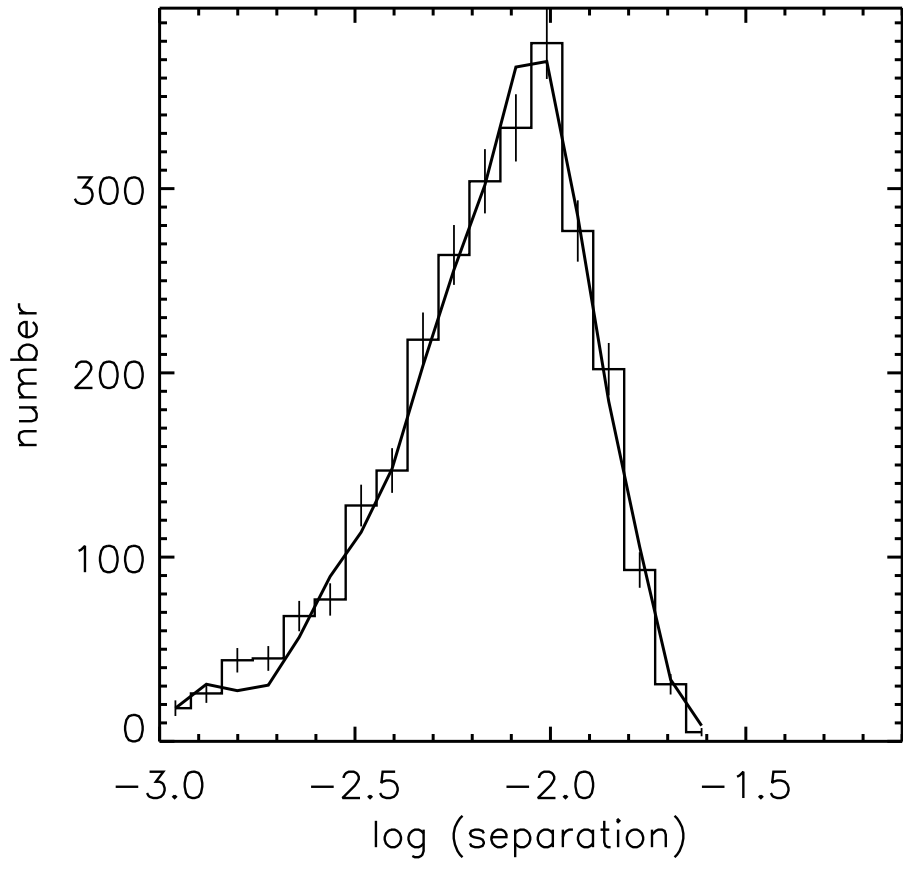
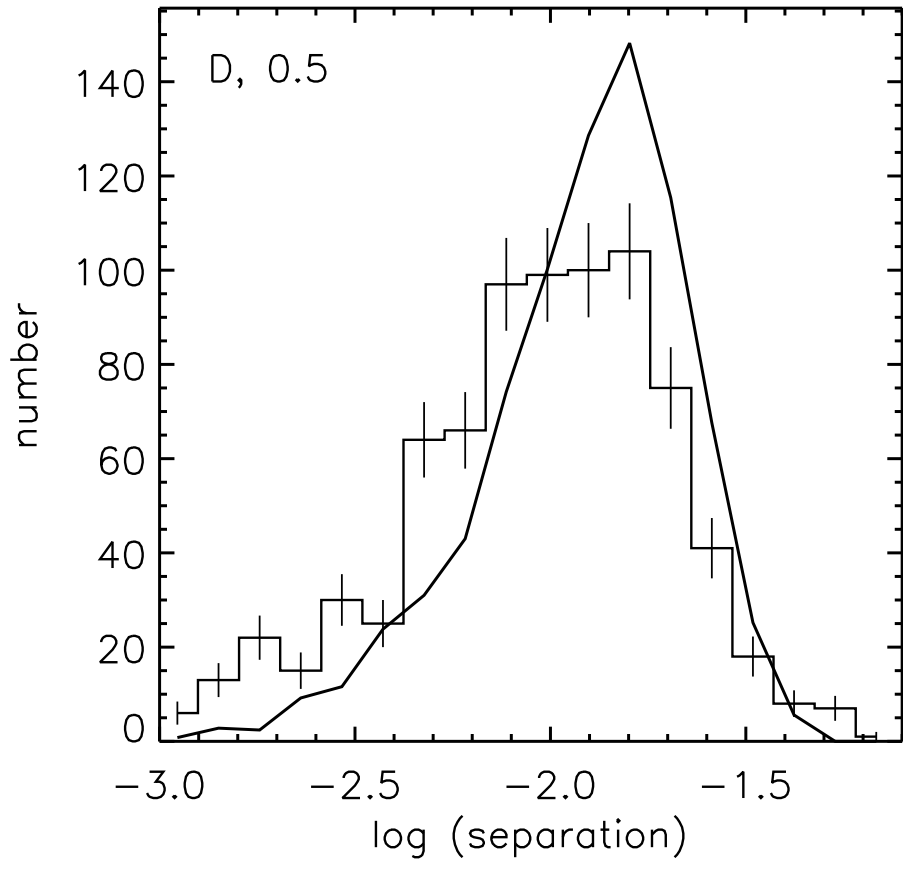


Fig.4





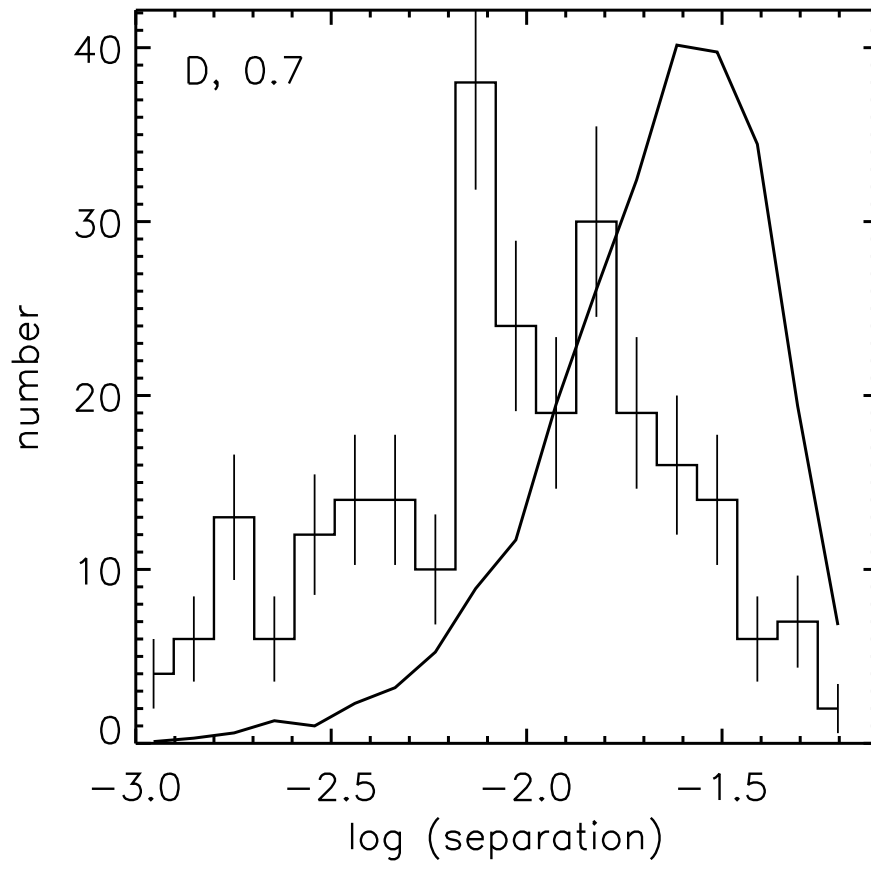


Fig.5

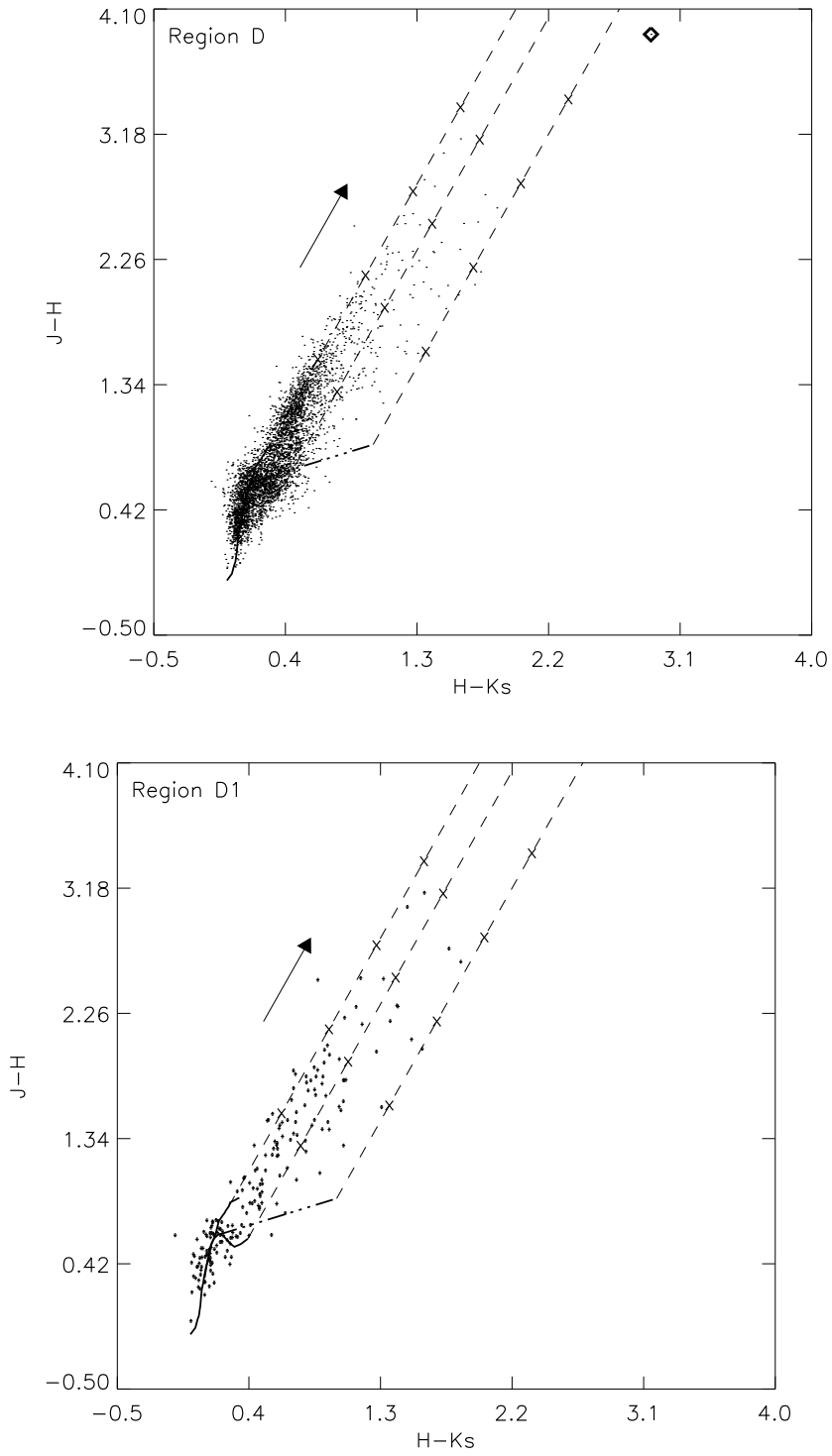


Fig.6

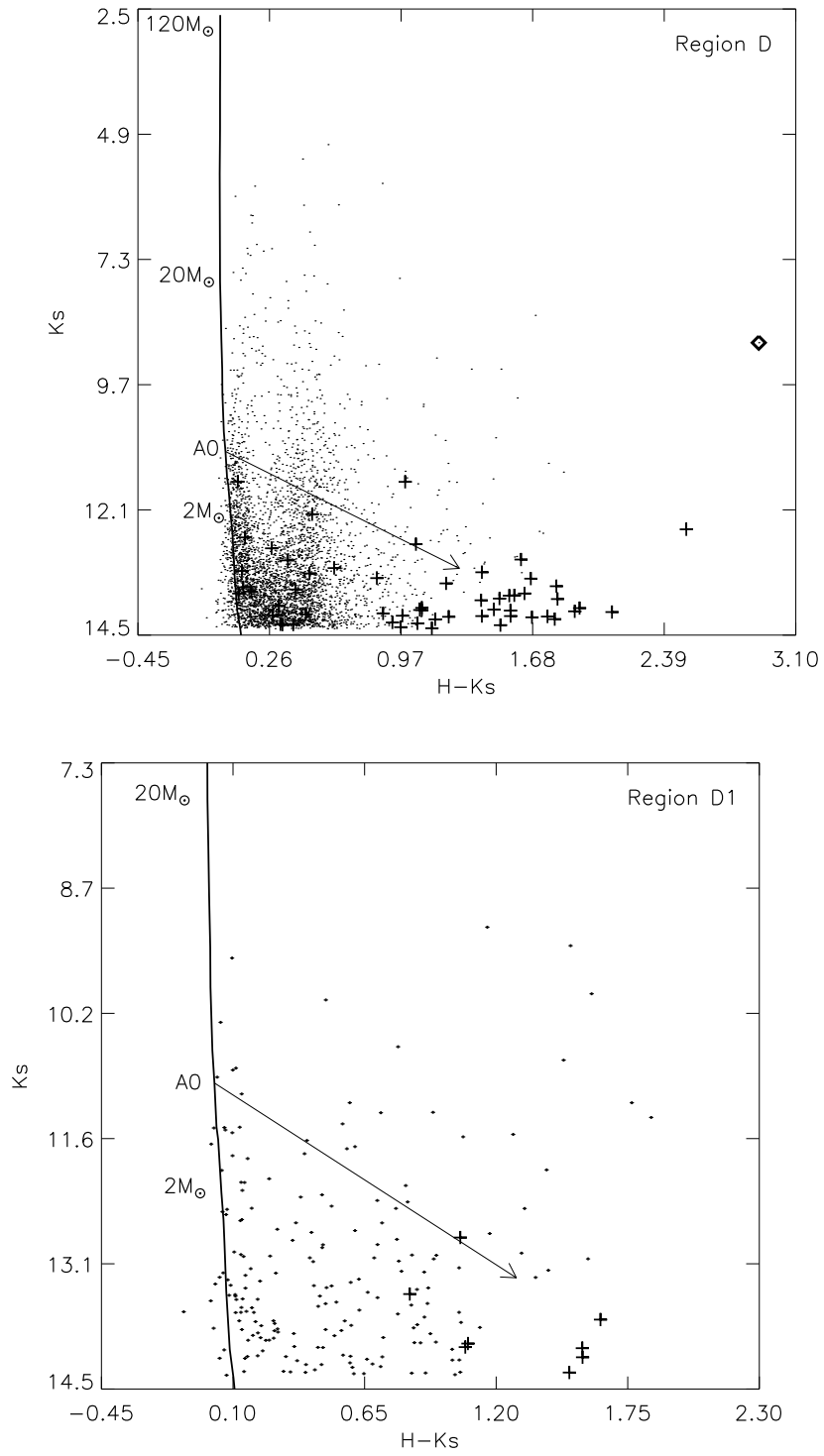


Fig.7

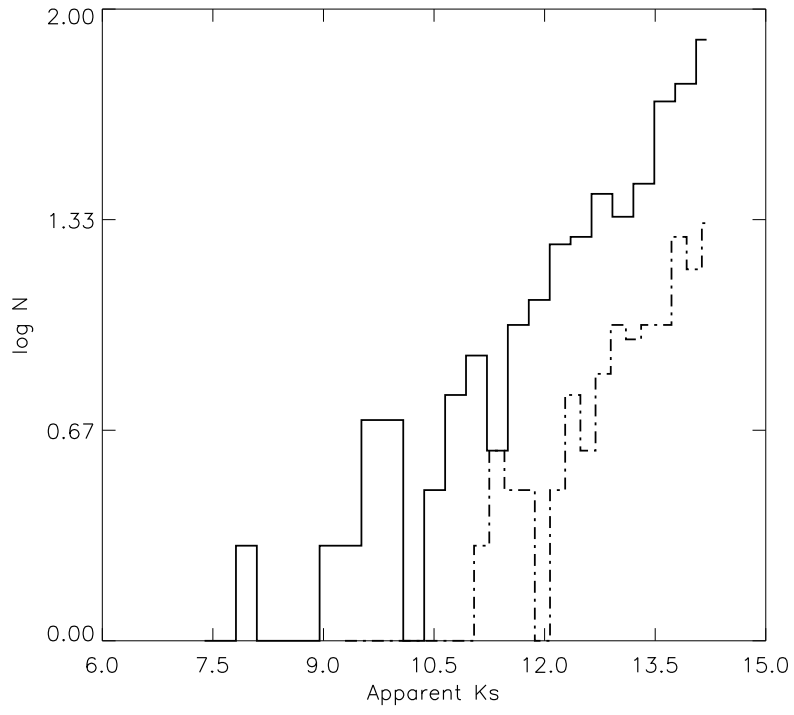


Fig.8

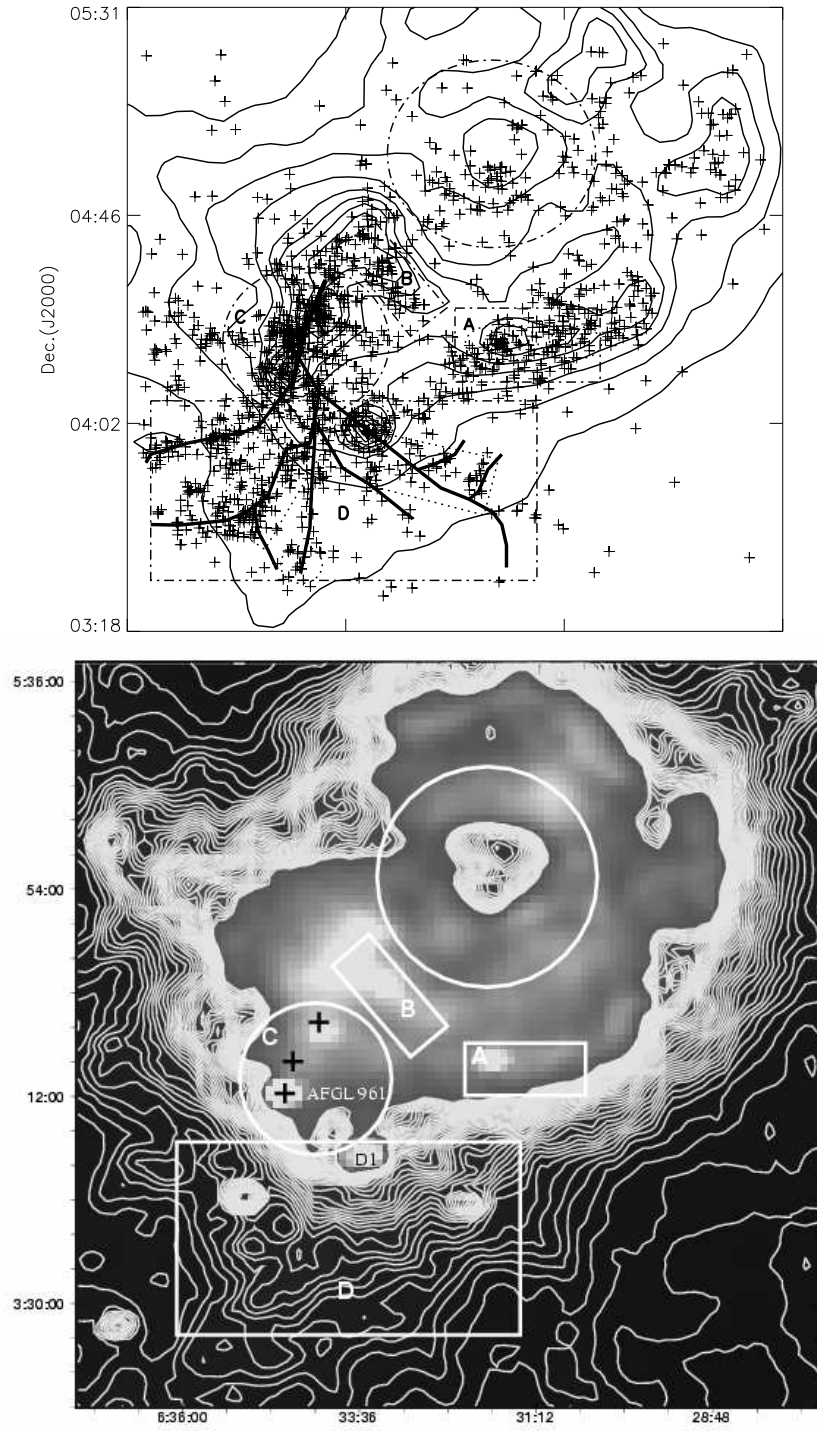


Fig.9